Pharmaceutical Research (2022) 39:1575–1586
https://doi.org/10.1007/s11095-022-03189-y

RESEARCH PAPER

In Vitro-In Vivo Correlation of Blood–Brain Barrier Permeability of Drugs: A Feasibility Study Towards Development of Prediction Methods for Brain Drug Concentration in Humans

Ryo Ito[1] · Hanae Morio[2] · Tomoyo Baba[2] · Yasuyuki Sakaguchi[2] · Naomi Wakayama[3] · Ryuto Isogai[2] · Yoshiyuki Yamaura[4] · Takafumi Komori[3] · Tomomi Furihata[2]

Received: 29 November 2021 / Accepted: 3 February 2022 / Published online: 14 March 2022

Abstract

Purpose *In vitro* human blood–brain barrier (BBB) models in combination with central nervous system-physiologically based pharmacokinetic (CNS-PBPK) modeling, hereafter referred to as the "BBB/PBPK" method, are expected to contribute to prediction of brain drug concentration profiles in humans. As part of our ongoing effort to develop a BBB/PBPK method, we tried to clarify the relationship of *in vivo* BBB permeability data to those *in vitro* obtained from a human immortalized cell-based tri-culture BBB model (hiBBB), which we have recently created.

Methods The hiBBB models were developed and functionally characterized as previously described. The *in vitro* BBB permeabilities (Pe, $\times 10^{-6}$ cm/s) of seventeen compounds were determined by permeability assays, and *in vivo* BBB permeabilities (Q_{ECF}) for eight drugs were estimated by CNS-PBPK modeling. The correlation of the Pe values with the Q_{ECF} values was analyzed by linear regression analysis.

Results The hiBBB models showed intercellular barrier properties and several BBB transporter functions, which were enough to provide a wide dynamic range of Pe values from 5.7 ± 0.7 (rhodamine 123) to 2580.4 ± 781.9 (rivastigmine). Furthermore, the *in vitro* Pe values of the eight drugs showed a good correlation ($R^2 = 0.96$) with their *in vivo* Q_{ECF} values estimated from human clinical data.

Conclusion We show that *in vitro* human BBB models provide clinically relevant BBB permeability that can be used as input for CNS-PBPK modeling. Therefore, our findings will encourage the development of a BBB/PBPK method as a promising approach for predicting brain drug concentration profiles in humans.

Keywords Blood–brain barrier · Central nervous system · Drug development · Immortalized cell · Physiologically based pharmacokinetic modeling

✉ Tomomi Furihata
tomomif@toyaku.ac.jp

[1] Research Center of Neurology, Ono Pharmaceutical Co., Ltd., Osaka, Japan

[2] Laboratory of Clinical Pharmacy & Experimental Therapeutics, School of Pharmacy, Tokyo University of Pharmacy and Life Sciences, 1432-1 Horinouchi, Hachioji, Tokyo 192-0392, Japan

[3] Global Drug Metabolism and Pharmacokinetics Tsukuba, Tsukuba Research Laboratories, Eisai Co., Ltd., Ibaraki, Japan

[4] Pharmacokinetic Research Laboratories, Ono Pharmaceutical Co., Ltd., Osaka, Japan

Abbreviations

BBB	Blood-brain barrier
CNS	Central nervous system
HBMEC	Human brain microvascular endothelial cells
HASTR	Human astrocytes
HBPC	Human brain pericytes
prHBMEC	Primary human BMEC
hprBBB	Primary HBMEC-based BBB models
hiBBB	Human immortalized cell-based BBB models
tsSV40T	Temperature sensitive simian virus 40 large tumor-antigen
SLC	Solute carrier
ABC	ATP Binding Cassette
P-gp	P-glycoprotein

BCRP	Breast cancer resistance protein
LAT1	L-type amino acid transporter 1
H^+/OC antiporter	Proton/organic cation antiporter
VE-cadherin	Vascular endothelial-cadherin
ZO-1	Zonula occludens 1
JAM-A	Junctional adhesion molecule A
GLUT1	Glucose transporter 1
TfR	Transferrin receptor
FcRn	Neonatal Fc receptor
INSR	Insulin receptor
MFSD2A	The major facilitator superfamily domain containing 2A
qPCR	Quantitative real-time PCR
GAPDH	Glyceraldehyde 3-phosphate dehydrogenase
TEER	Trans-endothelial electrical resistance
LY	Lucifer yellow
R123	Rhodamine123
CysA	Cyclosporin A
ER	Efflux ratio
Pe	Permeability coefficient
IVIVC	*In vitro-in vivo* Correlation
$f_{u,p}$	Drug unbound fraction in the plasma
NONMEM	Non-linear mixed effect model
ECF	Extracellular fluid
LV	Lateral ventricle
TFV	Third and fourth ventricle
CM	Cisterna magna
SAS	Subarachnoid space
CSF	Cerebrospinal fluid
PK	Pharmacokinetics
PPK	Population PK
PBPK	Physiologically based pharmacokinetics
LC–MS/MS	Liquid chromatography with tandem mass spectrometry

Introduction

The development of drugs for the treatment of central nervous system (CNS) diseases has long been challenging because of the presence of the blood–brain barrier (BBB), which makes difficult the accurate estimation of drug concentration in the human brain, a target site (1). The BBB is primarily formed by brain microvascular endothelial cells (BMEC) with the support of astrocytes and pericytes, where intercellular (tight/adherens) junctions and efflux transporters, such as P-glycoprotein (P-gp) and breast cancer resistance protein (BCRP) (2), are expressed to respectively establish physical and active barriers to drug entrance into the brain from the circulation. On the other hand, nutrient uptake transporters, like L-type amino acid transporter 1 (LAT1) and proton/organic cation antiporter (H^+/OC antiporter), are also expressed to serve as influx transporters at the BBB (3). These specialized BBB properties often result in disparate drug concentrations between plasma and brain (more specifically, brain extracellular fluid); the difference, however, cannot be solely explained by the physicochemical properties of the drugs, because the unbiased drug concentrations can be compromised by biological factors. Considering that direct measurement of brain drug concentration is practically impossible, development of a sophisticated method of brain drug concentration prediction from its systemic pharmacokinetic profile is necessary to design an appropriate regimen based on pharmacokinetic-pharmacodynamic theory.

To that end, physiologically based pharmacokinetic (PBPK) modeling is widely acknowledged as a promising approach. Several CNS-PBPK models consisting of empirical systemic compartments as well as multiple CNS compartments have recently been proposed (4), and, to enhance their predictive ability, the models often utilize BBB permeability parameters obtained from animal *in vivo* PK data, in silico physicochemical data, and/or *in vitro* permeability data using non-BMEC cells (*e.g.*, Caco-2 cells or individual transporter-overexpressing cells). However, animal data always pose the risk of false negative or positive prediction resulting from species differences (5), and in silico physicochemical data alone are inappropriate as mentioned earlier. In addition, use of the non-BMEC cells is controversial due to the difference in cellular structures and transporter expression profiles between BMEC and non-BMEC cells (6). Therefore, for easier and more accurate prediction, *in vitro* human BBB models are expected to become a promising alternative and provide credible surrogate parameters of *in vivo* BBB permeability to be incorporated into CNS-PBPK modeling. However, there has been no report directly addressing the concept validity and feasibility of this approach.

We have previously developed a human immortalized cell-based tri-culture type BBB model (hiBBB) (7). The hiBBB model shows essential barrier properties, including efflux transporter functions and, importantly, can distinguish between the BBB-permeable and non-permeable properties of ten selected compounds (7). Furthermore, the immortalization properties of the cells confer scalability and robustness to the model, which are extremely beneficial to the drug development process. Thus, the hiBBB model is considered a representative human BBB model for use in exploration of a new approach for predicting brain drug concentration profile through combination with CNS-PBPK modeling. However, the hiBBB model is still in the middle of functional characterization and its potential for application to the new approach remains to be seen.

Therefore, as an initial part of the proof-of-concept validation of a BBB model/CNS-PBPK combinatory prediction method for brain drug concentration profiles, we tried to

clarify whether the hiBBB models have the ability to provide BBB permeability parameters of drugs that are relevant to those found *in vivo*, which are estimated by using authentic CNS-PBPK modeling with human clinical data. Furthermore, to obtain a biological rationale behind this examination, we expanded functional characterization of the hiBBB model while comparing it with the primary HBMEC-based model.

Materials and methods

Cells and their culture methods

Human brain microvascular endothelial cells (BMEC)/conditionally immortalized clone 18 (HBMEC/ci18), human astrocytes/conditionally immortalized clone 35 (HASTR/ci35), and human brain pericytes/conditionally immortalized clone 37 (HBPC/ci37), which were developed in our previous works (7–9), were cultured as described therein. These cells carry temperature-sensitive simian virus large T antigen (tsSV40T) and human telomerase catalytic subunit as immortalization genes. The tsSV40T functions allowed the cells to change their status from proliferation to differentiation by switching the culture temperature (33°C to 37°C). For more details regarding the characteristics of immortalized cells, please see our previous reports (7, 9–11).

Cryopreserved primary human BMEC (prHBMEC, normal human brain cortex-derived) were purchased from Cell Systems (Kirkland, WA, USA) (lot numbers 376.02.03.21.2F and 376.03.04.01.2F) and cultured at 37°C with 5% CO_2/95% air in the same medium as HBMEC/ci18 cells. The passage number of prHBMEC cells used for the permeability assays was 4, and those used for the mRNA analyses were from 5 to 7. All culture dishes were coated with type-I collagen.

Development of *in vitro* human BBB tri-culture models

The hiBBB model was developed by combining the three types of human immortalized BBB cells in the transwell culture system (12-well type, translucent polyethylene terephthalate, 0.4 μm high-density pores, BD Falcon, Franklin Lakes, NJ, USA, cat# 353494) using the same protocol as described previously (7). The procedure for development of the primary HBMEC-based models (hprBBB) was essentially the same as the hiBBB model except that HBMEC/ci18 cells were replaced by prHBMEC and the culture temperature in step 3 was set to 37°C. The schematic illustration in Fig. 2a provides an overview of the setup protocol of these models.

Total RNA isolation, cDNA synthesis, and quantitative real-time PCR (qPCR)

The total RNA extraction, genome DNA contamination check, and cDNA synthesis were performed as described previously (11). The qPCR was conducted using cDNA with the primers listed in Table S1. The target mRNAs are shown in the figure legends. The amplification efficiency of each qPCR was confirmed to be close to one. The expression data were normalized to the expression level of glyceraldehyde 3-phosphate dehydrogenase (GAPDH) mRNA.

RNA-sequencing and data analysis

The total RNA of prHBMEC and HBMEC/ci18 (200 ng each) were used for RNA-sequencing (which was done by Genewiz, Tokyo, Japan). After passing the quality check, the RNAs were subjected to cDNA library construction using a NEBNext Ultra II RNA Library Prep Kit for Illumina (New England BioLabs, MA, USA). RNA sequencing with a paired-end sequencing length of 150 bp was carried out on the Illumina NovaSeq 6000 platform (Illumina, Inc., San Diego, CA, USA). The RNA-sequence reads were aligned by GRCh38 (hg38), and gene expression levels were quantified using HTSEQ v0.6.1. Valid mRNA expression levels for comparison analyses were designated as the fragments per kilobase of exon per million mapped reads (FPKM) value > 5.

Determination of transendothelial electrical resistance (TEER)

TEER measurement was performed using the Millicell ERS-2 (Millipore, Darmstadt, Germany) with STX01 electrode (Millipore) according to the manufacturer's instructions. The culture insert areas were used to calculate TEER values ($\Omega \times cm^2$).

In vitro BBB permeability assays

Drug and compound permeability assays were performed using the hiBBB or hprBBB models. After rinsed once with Dulbecco's phosphate-buffered saline containing calcium and magnesium (Thermo Fisher Scientific, Waltham, MA, USA), the cells cultured on inserts were pre-incubated with Hanks' balanced salt solution with calcium and magnesium (Thermo Fisher Scientific) at 33°C (for the hiBBB model) or 37°C (for the hprBBB model) for 10 min, respectively. The temperature was then shifted to 37°C, and each test compound was added to the apical side of each insert to start the assays. The compounds were: rivastigmine (Namiki Shoji, Tokyo, Japan), carbamazepine (Sigma, St. Louis, MO, USA), memantine (Sigma), diphenhydramine (Sigma),

donepezil (Wako, Osaka, Japan), efavirenz (Tokyo Chemical Industry, Tokyo, Japan), phenytoin (Wako), indomethacin (Wako), risperidone (Wako), gabapentin (Toronto Research Chemicals, Toronto, Ontario, Canada), atenolol (Tokyo Chemical Industry), vancomycin (Wako), methotrexate (Sigma), cefotaxime (Combi-Blocks, San Diego, CA, USA), lucifer yellow (LY, Sigma), rhodamine123 (R123, Wako), and dantrolene (Wako). Their concentration was set at 1 μM except for R123 and dantrolene (5 μM). After incubation for 30, 60, and 90 min at 37°C, the medium was collected from the basolateral side of each insert for determination of compound concentration.

Inhibition analysis of P-gp, BCRP, and H^+/OC antiporter were performed using their respective specific inhibitors or competitive substrate. The P-gp and BCRP inhibitors were cyclosporin A (CysA, Tokyo Chemical Industry, 10 μM) and Ko143 (Sigma, 1 μM), respectively. The competitive substrate for H^+/OC antiporter was pyrilamine (Sigma, 1 mM). These inhibitors and competitor were added to both the apical and basolateral chambers. After pre-incubation for 2 h, the permeability assays were performed according to the method described above.

The fluorescence intensities of LY and R123 were determined using a SpectraMax microplate reader (Molecular Devices, San Jose, CA, USA) with excitation/emission wavelengths (nm) setting at 428/536 for LY and 505/534 for R123. For other compounds, quantitative analyses were performed using a QTRAP 5500 LC–MS/MS system (AB Sciex, Framingham, MA, USA). Loaded samples were separated on an Atlantis T3 column (100 Å, 3 μm, 2.1 mm × 50 mm, Waters, Milford, MA, USA). The mobile phases consisted of (A) water with 0.1% (v/v) formic acid and (B) acetonitrile with 0.1% (v/v) formic acid. The m/z information are described in Table S2.

The permeability coefficient (Pe, $\times 10^{-6}$ cm/s) of each compound was calculated as described previously (7). The cleared volume was calculated from the concentration of the compounds on the apical (C_{apical}) or basolateral ($C_{basolateral}$) side of the insert and the volume on the apical (V_{apical}; 750 μL) or basolateral side ($V_{basolateral}$; 2250 μL) by the following equation:

$$Clearedvolume_{AtoB}(\mu L) = \frac{C_{basolateral} \times V_{basolateral}}{C_{apical}}$$

$$Clearedvolume_{BtoA}(\mu L) = \frac{C_{apical} \times V_{apical}}{C_{basolateral}}$$

After the cleared volume was plotted versus time, the slope of the clearance curve for BBB models (PS_{total}) and for the cell-free insert (PS_{insert}) were calculated, respectively, and the permeability × area product value for the endothelial monolayer (PS_e) was determined by the following equation:

$$\frac{1}{PS_e} = \frac{1}{PS_{total}} - \frac{1}{PS_{insert}}$$

Finally, the Pe value was determined by dividing the PS_e value by the surface area (A; 0.9 cm^2 for 12-well insert) as follows:

$$Pe = \frac{PS_e}{A}$$

In the bi-directional transport assays examining P-gp and BCRP functions, the efflux ratios were determined by dividing the Pe values in the basolateral-to-apical direction by that in the apical-to-basolateral direction (Pe_{BA}/Pe_{AB}).

Human central nervous system (CNS) – physiologically based pharmacokinetics (PBPK) modeling

The CNS-PBPK model was constructed based on a previous report (4) with slight modifications as shown in Fig. 5a. Either a 1- or 2-compartment model was applied to fit the PK of each drug. The basic PK parameters were as follows: the first-order absorption rate constant (K_a), total clearance (CL), volume of distribution for the central compartment (V_c) and peripheral compartments (V_1), and intercompartmental clearance (Q_1).

Population PK (PPK) analysis with the non-linear mixed effect model (NONMEM) was performed using NONMEM version 7.3 (subroutines ADVAN 13; ICON Development Solutions, Hannover, MD, USA). The first-order conditional estimation method with interaction (FOCEI) was used for parameter estimation. The differential equations are as follows:

$$\frac{dA_{gut}}{dt} = -K_a \times A_{dose} \quad (1)$$

$$V_c \bullet \frac{dC_{Vc}}{dt} = K_a \times A_{dose} - \frac{(Q_1 + CL + Q_{ECF})}{V_c} \times f_{u,p} \times A_{Vc} + \frac{Q_1}{V_1} \times A_{V1} \times f_{u,p} + \frac{Q_{diff}}{V_{SAS}} \times A_{SAS} \quad (2)$$

$$V_1 \bullet \frac{dC_{V1}}{dt} = \frac{Q_1}{V_c} \times A_{Vc} \times f_{u,p} - \frac{Q_1}{V_1} \times A_{V1} \times f_{u,p} \quad (3)$$

$$V_{ECF} \bullet \frac{dC_{ECF}}{dt} = \frac{Q_{ECF}}{V_c} \times A_{Vc} \times f_{u,p} - \frac{Q_{diff}}{V_{ECF}} \times A_{ECF} \quad (4)$$

$$V_{LV} \bullet \frac{dC_{LV}}{dt} = \frac{Q_{diff}}{V_{ECF}} \times A_{ECF} - \frac{Q_{diff}}{V_{LV}} \times A_{LV} \quad (5)$$

$$V_{TFV} \bullet \frac{dC_{TFV}}{dt} = \frac{Q_{diff}}{V_{LV}} \times A_{LV} - \frac{Q_{diff}}{V_{TFV}} \times A_{TFV} \quad (6)$$

$$V_{CM} \bullet \frac{dC_{CM}}{dt} = \frac{Q_{diff}}{V_{TFV}} \times A_{TFV} - \frac{Q_{diff}}{V_{CM}} \times A_{CM} \quad (7)$$

$$V_{SAS} \bullet \frac{dC_{SAS}}{dt} = \frac{Q_{diff}}{V_{CM}} \times A_{CM} - \frac{Q_{diff}}{V_{SAS}} \times A_{SAS} \quad (8)$$

where C and A represent the concentration and amount of each drug, respectively; V_C and V_1 represent the volumes of distribution for the central compartment and peripheral compartment, respectively; Q_1 represents the intercompartmental clearance between the central (V_c) and peripheral compartment (V_1); Q_{ECF} and Q_{diff} are the CNS drug-specific parameters representing the clearance from the central compartment to the brain extracellular fluid ($Brain_{ECF}$), and the diffusion rate in the brain and CSF, respectively; and V_{LV}, V_{TFV}, V_{CM}, and V_{SAS} are system-specific (physiological) parameters representing the volume of CSF in the lateral ventricle (LV), third and fourth ventricle (TFV), cisterna magna (CM), and subarachnoid space (SAS), respectively. The system-specific parameters in humans are summarized in Table I.

The interindividual variability of PK parameters was modeled according to an exponential equation as follows:

$$\theta_i = \theta \bullet exp(\eta_i) \quad (9)$$

where θ is the population parameter value; θ_i is the individual parameter; and η_i represents the random effect of mean zero and variance ω^2. The following proportional error model was described as the residual error:

$$C_{ij} = \Upsilon_{PRED,ij} \times (1 + \varepsilon_{ij}) \quad (10)$$

where $\Upsilon_{PRED,ij}$ represents the jth concentration in individual i predicted by the PK model and C_{ij} is the observed concentration. Values of ε_{ij} are assumed to be independently and normally distributed with mean zero and variance σ^2.

Table I System-specific parameters used in CNS-PBPK modeling

Parameters	Human	References
$Brain_{ECF}$ (mL)	260	(4, 12)
V_{LV} (mL)	22.5	(4, 12)
V_{TFV} (mL)	22.5	(4, 12)
V_{CM} (mL)	7.5	(4, 12)
V_{SAS} (mL)	107.5	(4, 12)

$Brain_{ECF}$, brain extracellular fluid; V_{LV}, volume of CSF in the lateral ventricle; V_{TFV}, volume of CSF in the third and fourth ventricle; V_{CM}, volume of CSF in the cisterna magna; V_{SAS}, volume of CSF in the subarachnoid space

Simulations were performed 500 times to obtain the 5th, 50th, and 95th percentiles. Evaluation of NONMEM outputs and graphical analyses were performed using Excel 2010 (Microsoft, Redmond, WA, USA).

Statistical analysis

Statistical analysis was performed using Excel with ystat2006 (Igakutosho Shuppan Ltd, Tokyo, Japan). Comparisons between two values were performed by using the unpaired Student t-test.

Results

Comprehensive characterization of gene expression profiles in HBMEC/ci18 cells

First, we tried to obtain the comprehensive gene expression profile of HBMEC/ci18 cells for comparison to that of prHBMEC with the expectation that their similarity would imply that HBMEC/ci18 cells have essential BBB characteristics. RNA-sequencing analyses found that overall similarity (defined as differences within 1/3 ~ threefold) in their gene expression profiles was as high as 97.6% (6203/6359 of mRNAs examined). Even when focused on subsets of BBB-enriched mRNAs, the similarities were still very high: 84.6% (11/13) for tight-junction proteins, 100% (9/9) for receptors, 90.9% (10/11) for SLC transporters, and 90.0% (9/10) for ABC transporters, respectively (Fig. 1a). The target genes used in the analyses are listed in Table S3.

In addition, we validated the similarities in the expression of several BBB-enriched genes between the two cell types by qPCR. With few exceptions, the mRNA expression levels of the BBB-enriched genes in HBMEC/ci18 cells were roughly comparable to those in prHBMEC, suggesting that HBMEC/ci18 cells retain the fundamental BBB gene expression profile (Fig. 1b).

Characterization of BBB functionalities of the hiBBB model

To seek additional reasons to use HBMEC/ci18 cells for the development of a human BBB model, we compared the essential BBB functionalities of the hiBBB and the hprBBB models. These models were developed according to the culture protocols shown in Fig. 2a.

In order to characterize the barrier properties of the models, TEER measurement and LY permeability assays were performed. The TEER of the hiBBB model was 106.7 ± 3.7 ($\Omega \times cm^2$), which was very close to that obtained from the hprBBB model ($99.6 \pm 2.6\ \Omega \times cm^2$). Likewise, the LY permeability coefficients (Pe, $\times 10^{-6}$ cm/s) obtained from the

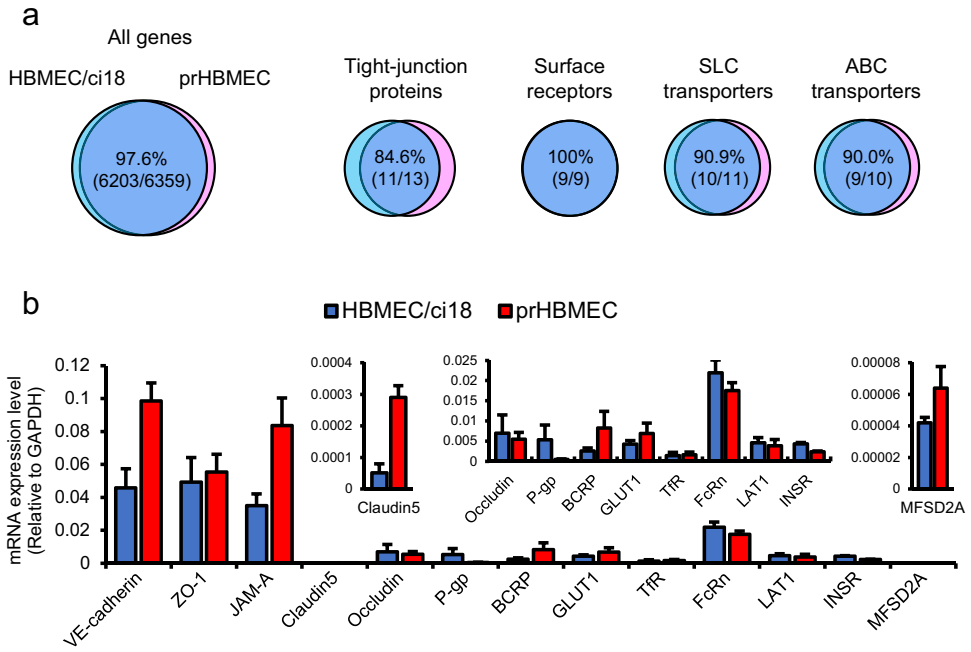

Fig. 1 Characterization of gene expression profiles in HBMEC/ci18 cells and primary HBMEC (**a**) RNA-sequencing analyses were performed to compare differences in gene expression profiles between HBMEC/ci18 and prHBMEC cells. Among mRNAs identified, those carrying the FPKM value above 5 were picked up and used in comparison analyses, and "the similar gene expression level" between the two cell types was defined as its difference within the 1/3 ~ threefold range. Based on the results, the Venn diagrams were depicted for all pickup genes, as well as subsets of BBB-enriched genes (tight-junction proteins, surface receptors, SLC transporters, and ABC transporters), to visualize the degree of the overall gene expression similarities between the two types of the cells (indicated by the merged areas). The gene numbers identified/examined are also shown. The list of genes used in subsets analyses are summarized in Table S3. (**b**) The mRNA expression levels of BMEC-enriched genes in HBMEC/ci18 and prHBMEC cells were validated using quantitative real-time PCR (qPCR). The targets are vascular endothelial-cadherin (VE-cadherin), zonula occludens 1 (ZO-1), Junctional adhesion molecule A (JAM-A), claudin-5, occludin, P-glycoprotein (P-gp), breast cancer resistance protein (BCRP), glucose transporter 1 (GLUT1), transferrin receptor (TfR), neonatal Fc receptor (FcRn), L-type amino acid transporter 1 (LAT1), insulin receptor (INSR), and the major facilitator superfamily domain containing 2A (MFSD2A). The values were normalized to glyceraldehyde 3-phosphate dehydrogenase (GAPDH) mRNA levels, and the results are shown as the mean ± SEM obtained from three independent experiments. Each experiment was performed in duplicate.

hiBBB and the hprBBB models were comparable (27.7 ± 4.2 and 31.1 ± 3.7, respectively) (Figs. 2b and 2c).

Then, to examine the efflux transporter functions of the hiBBB and the hprBBB models, the bi-directional transport assays were performed using R123 (a P-gp substrate) and dantrolene (a BCRP substrate). The results showed that the efflux ratios of both R123 (2.0 ± 0.17) and dantrolene (1.9 ± 0.19) in the hiBBB model were comparable to those of the hprBBB model (2.6 ± 0.44 for R123, and 1.5 ± 0.60 for dantrolene) (Figs. 2d and 2e). Moreover, pre-treatment with CysA (a P-gp inhibitor) or Ko143 (a BCRP inhibitor) resulted in significant decreases of the efflux ratios in the hiBBB model (0.63 ± 0.26 for R123, and 0.79 ± 0.20 for dantrolene) and in the hprBBB model (0.71 ± 0.09 for R123, and 0.59 ± 0.11 for dantrolene) (Figs. 2d and 2e). Collectively, these data indicate the functional expression of P-gp and BCRP in both BBB models.

To further gain functional insights, we examined the activity of H^+/OC antiporter, as yet unidentified genetically but surely functional as a drug influx transporter at the BBB (3), in the hiBBB model using its antiporter substrates (Fig. 3). In the permeability assays, the Pe values of memantine and diphenhydramine were 715.6 ± 164.8 and 702.6 ± 153.4, respectively. Furthermore, in the competitive inhibition assays using pyrilamine (another H^+/OC antiporter substrate), the Pe values were substantially reduced to 9.3 ± 5.9 (memantine) and 25.5 ± 0.8 (diphenhydramine), respectively. These results indicate that H^+/OC antiporter is functionally expressed in the hiBBB model.

Taken all together, these results strongly emphasize that the hiBBB model possesses both physical barrier properties and influx and efflux transporter functions.

In vitro BBB permeability assays

Given that the hiBBB model has the functional BBB properties, we then moved forward on *in vitro-in vivo* correlation (IVIVC) analyses to assess whether *in vitro* human BBB models can provide useful BBB permeability data for predicting brain drug concentration profile through combination with CNS-PBPK modeling.

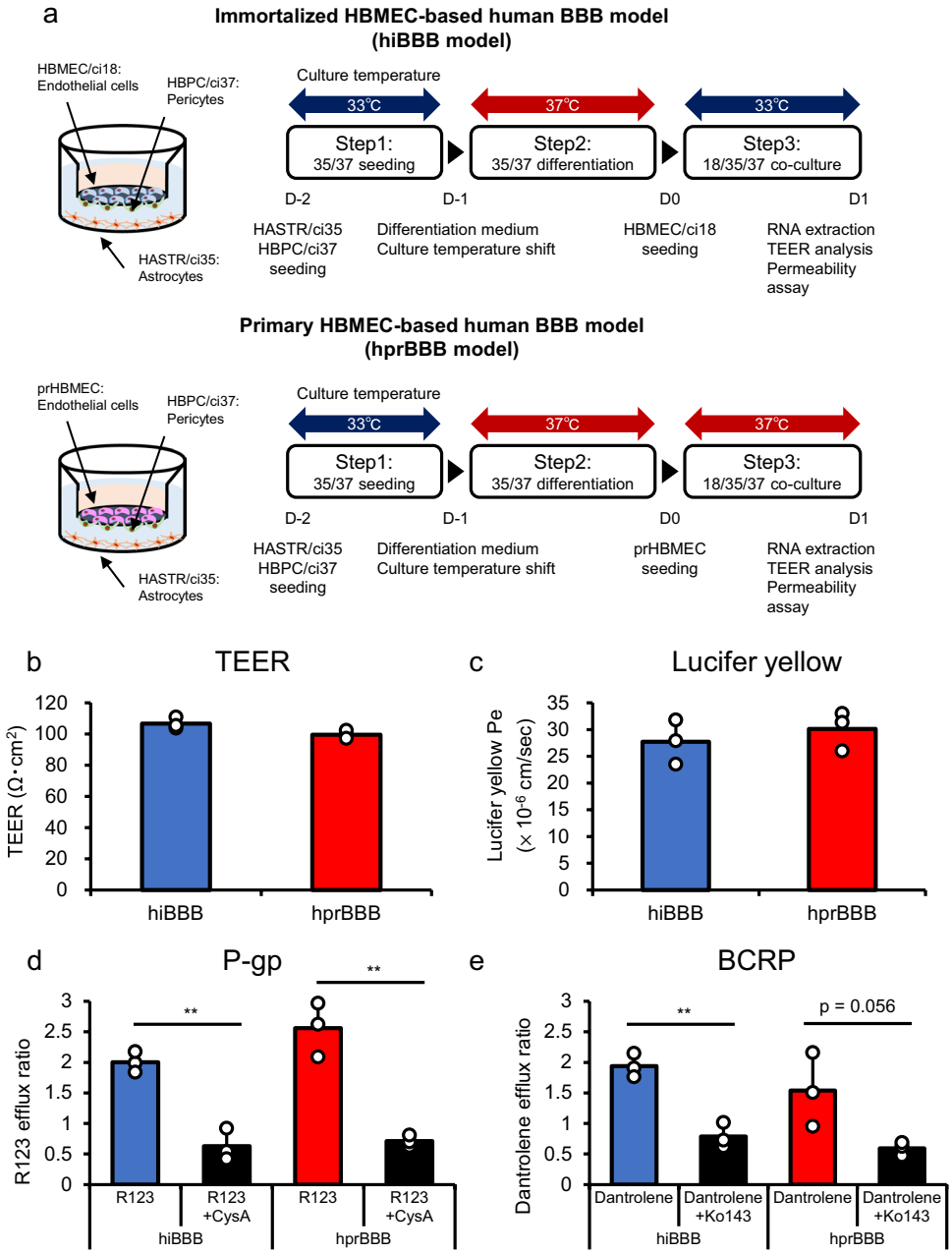

Fig. 2 Characterization of the BBB functionalities in the hiBBB and the hprBBB models (**a**) Schematic drawings are shown to provide an overview of the development of the hiBBB and the hprBBB models in a 12-well transwell culture system. Additional notes are: the membranes of cell culture inserts (translucent polyethylene terephthalate, 0.4 μm high-density pores, BD Falcon, cat#353494) were incubated with 100 μg/mL type-IV collagen/100 μg/mL fibronectin solution at 37°C for one hour (extracellular matrix coating). The inserts were dried by air and rinsed with phosphate-buffered saline twice. (**b**) and (**c**) The trans-endothelial electrical resistance (TEER) and the lucifer yellow (LY) permeability coefficient (Pe) values were measured in both BBB models on day 1 of co-culturing. (**d**) and (**e**) The bi-directional transport assays with 5 μM rhodamine123 (R123) (a P-gp substrate) and 5 μM dantrolene (a BCRP substrate) were performed using both BBB models. The efflux ratios (ER) were obtained by the equation: $ER = Pe_{BA}/Pe_{AB}$, where the Pe_{AB} and Pe_{BA} values were permeability coefficients (from the apical to the basolateral direction and vice versa, respectively). Validation of the P-gp and BCRP functions was performed using their specific inhibitors (10 μM cyclosporine A [CysA] and 1 μM Ko143, respectively). Each value represents the mean ± SD obtained from three independent experiments, each performed in duplicate. **, $p < 0.01$. Each dot represents the individual value obtained.

To begin with, we performed drug BBB permeability studies using seventeen model compounds or drugs. Briefly, they include the influx transporter substrates (memantine, diphenhydramine, and gabapentin), P-gp substrates (risperidone, gabapentin, and R123), BCRP substrates (dantrolene and methotrexate), and LY, a non-permeable marker. The results showed that the hiBBB model clearly discriminated their BBB permeabilities, as the average

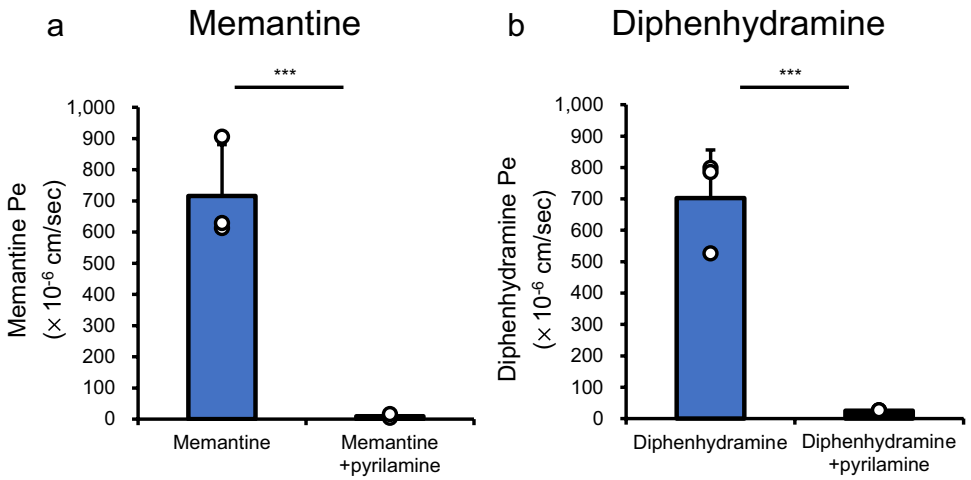

Fig. 3 Characterization of proton-coupled organic cation (H^+/OC) antiporter functions in the hiBBB model. Permeability assay with the H^+/OC antiporter substrates memantine (**a**) and diphenhydramine (**b**) were performed in the hiBBB models. Memantine (1 μM) or diphenhydramine (1 μM) were added to the insert chamber, followed by incubation for 30, 60, or 90 min. Concentration data were used to calculate Pe values (from the apical to the basolateral direction). In the competitive analysis, pyrilamine (1 mM) was used as a competitive inhibitor. Each value represents the mean ± SD obtained from three independent experiments, each performed in duplicate. ***, $p < 0.001$. Each dot represents the individual value obtained.

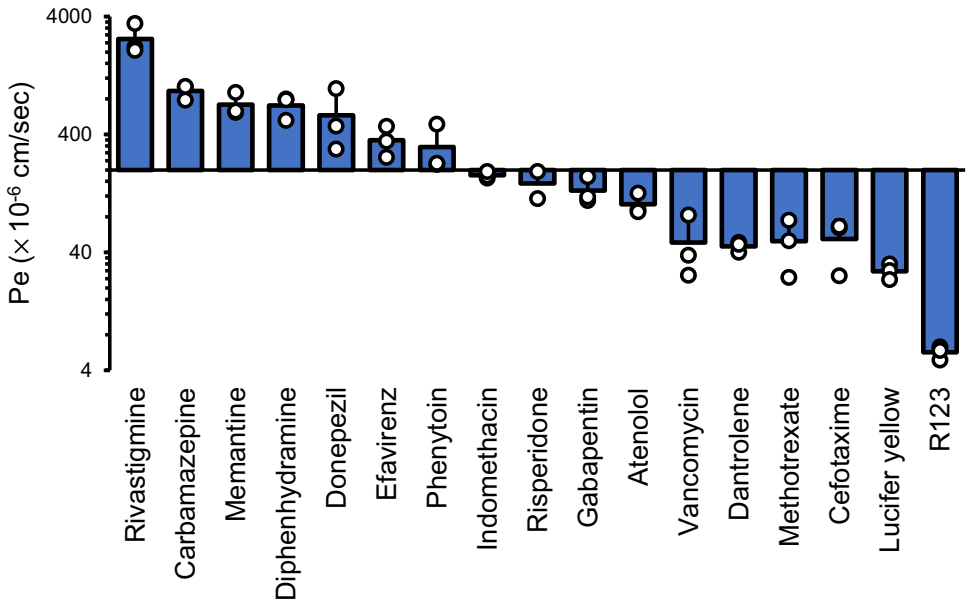

Fig. 4 Characterization of the BBB permeabilities of several drugs and compounds in the hiBBB model. The hiBBB model was used to assess BBB permeability to several drugs and compounds with differential BBB permeability profiles, including rivastigmine, carbamazepine, memantine, diphenhydramine, donepezil, efavirenz, phenytoin, indomethacin, risperidone, gabapentin, atenolol, vancomycin, dantrolene, methotrexate, cefotaxime, lucifer yellow, and R123. Among them, risperidone, gabapentin, and R123 are P-gp substrates, dantrolene and methotrexate are BCRP substrates, and memantine and diphenhydramine are H^+/OC antiporter substrates. The concentrations used were: 5 μM for R123 and dantrolene, and 1 μM for others. The Pe determination was performed as described in Figs. 2 and 3. Each value represents the mean (SD) obtained from three independent experiments. Each experiment was performed in duplicate. Each dot represents the individual value obtained

Pe value of the drugs with higher BBB permeabilities ($> 200 \times 10^{-6}$ cm/s, indicated by a horizontal line in Fig. 4) was 883.6 cm/s and that of the lower BBB permeable drugs or compounds was 79.9 cm/s. Rivastigmine and R123 showed the highest and the lowest Pe values (2580.4 ± 781.9, and 5.7 ± 0.7, respectively), indicating the large dynamic range of Pe values (more than 450-fold). The Pe values are summarized in Table II.

Table II List of the compounds used in the BBB permeability assays

Compounds	Pe ($\times 10^{-6}$ cm/s)
Rivastigmine	2580 ± 782
Propranolol[a]	1280 ± 686
Carbamazepine	935 ± 133
Memantine	716 ± 165
Diphenhydramine	703 ± 153
Donepezil	582 ± 352
Efavirenz	357 ± 106
Phenytoin	313 ± 153
Indomethacin	180 ± 11.8
Risperidone	153 ± 39.6
Gabapentin	134 ± 35.1
Atenolol	102 ± 21.3
Vancomycin	48.6 ± 30.0
Dantrolene	45.0 ± 4.48
Methotrexate	49.7 ± 25.0
Cefotaxime	52.0 ± 23.2
Lucifer yallow	27.7 ± 4.15
R123	5.69 ± 0.73

[a], The Pe values of propranolol used here had been determined in our previous study (7).

Estimation of *in vivo* BBB permeability using human CNS-PBPK modeling

Then, to obtain *in vivo* BBB permeability values to be used for a comparison with *in vitro* Pe data, we set up the CNS-PBPK model based on a previous report (4) with slight modifications as shown in Fig. 5a. Briefly, the CNS-PBPK model was constructed by combining empirical systemic compartments with physiologically based CNS multi-compartments, and the CNS system parameters used here are shown in Table I. The human clinical data reported in the literature are summarized in Table III, in which information on only eight out of the fifteen drugs tested in Fig. 4 were obtainable due to the lack of available reports for other seven drugs. The results of the visual predictive check showed that our CNS-PBPK model adequately described the drug concentration–time profiles (Fig. S1).

Under the above-described conditions, the *in vivo* drug-specific parameters of human BBB permeability (clearance from plasma to $Brain_{ECF}$: Q_{ECF}) were estimated. The resulting Q_{ECF} values are summarized in Table IV, along with other drug-specific parameters. As shown in Figure S2, several diagnostic plots (the population analysis-predicted *vs.* observed values, and conditional weighted residuals *vs.* population analysis-predicted values or time) validate the predictive accuracy of our CNS-PBPK models.

IVIVC analysis of human BBB permeability

Finally, we assessed the correlation level between the *in vitro* Pe values and the estimated *in vivo* Q_{ECF} values for the eight drugs in order to clarify the degree of their similarity (Fig. 5b) (Note that the Pe values of propranolol used here had been determined in our previous study (7)). The results showed that, while the methotrexate data-point stands slightly off, other drugs were in close proximity to the linear regression curve, making their coefficients of determination remarkably high ($R^2 = 0.96$). Therefore, the results clearly show that, at least for the eight drugs tested, the BBB permeability values obtained using the hiBBB model are comparable to those estimated *in vivo*.

Discussion

In vitro human BBB models in combination with CNS-PBPK modeling, which we refer to as the "BBB/PBPK" method, are expected to aid prediction of brain drug concentration profiles in humans. However, this methodology, including the benchmark functional requirements of *in vitro* human BBB models, remains to be established. To make a progress, we have taken the first step toward addressing the concept validity of a BBB/PBPK method using the hiBBB model as a representative *in vitro* human BBB model after

Table III Summary of the human clinical data

Compounds	Dosage	Number of samples	Age	Condition of patients	Sampling position	References
Cefotaxime	infusion	6	52—79	Uninflamed meninges	CSF_{SAS}	(13)
Efavirenz	p.o	80	36—52	HIV-1	CSF_{SAS}	(14)
Indomethacin	infusion	31	0.3—12	Healthy children	CSF_{SAS}	(15)
Gabapentin	p.o	5	22—38	Partial epilepsy	CSF_{SAS}	(16)
Methotrexate	infusion	1	40	Glioma	$Brain_{ECF}$	(17)
Phenytoin	infusion	6	25—60	Epilepsy	CSF_{SAS}	(18)
Propranolol	p.o	37	30—73	Diagnosis	CSF_{SAS}	(19)
Rivastigmine	p.o	18	45—85	Alzheimer's disease	CSF_{SAS}	(20)

Table IV Parameter estimates for eight drugs in CNS-PBPK modeling

Parameters	Cefotaxime	Efavirenz	Indomethacin	Gabapentin	Methotrexate	Phenytoin	Propranolol	Rivastigmine
$f_{u,p}$	0.71 (Ref. 21)	0.005 (Ref. 14)	0.1 (Ref. 15)	0.97 (Ref. 22)	0.48 (Ref. 21)	0.1 (Ref. 23)	0.064 (Ref. 24)	0.36 (Ref. 20)
K_a (h^{-1})	-	0.179 (0.000379)	-	0.420 (0.101)	-	-	0.119 (0.0344)	0.421 (0.16)
CL (L/h)	14.8	804 (1.14)	22.7 (3.82)	18.5 (3.13)	13.2 (0.0393)	151 (50.3)	1450 (234)	418 (69.5)
Q_1 (L/h)	43.5	-	46.6 (18.9)	9.59 (4.73)	10.7 (0.107)	-	-	9940 (1430)
Q_{ECF} (L/h)	0.00355	0.0978 (0.000146)	0.031 (0.00867)	0.00938 (0.00315)	0.00131 (0.00000305)	0.070 (0.0137)	0.443 (0.619)	0.871 (0.165)
Q_{diff} (L/h)	0.101	9.93 (0.000984)	1.05 (0.223)	6.42 (4.18)	0.0401 (0.0000299)	3.39 (0.560)	0.723 (0.334)	0.424 (0.0861)
V_c (L/h)	1.04	98.5 (0.151)	1.44 (0.439)	77.4 (13.0)	1.5 (0.00248)	29.4 (5.74)	1.63 (2.92)	0.530 (0.157)
V_1 (L/h)	15.6	-	1.93 (0.673)	76.4 (18.2)	9.4 (0.0628)	-	-	124 (72.1)

The parameters were estimated by NONMEM (subroutine ADVAN 13) using the plasma and CSF or ECF concentration–time profile of each drug in humans. The values in parentheses represent the relative standard error of the estimate.

its functional validation. Overall, our results support the feasibility of the new method for brain drug concentration prediction.

As stated in the introduction, BBB/PBPK methods are expected to have high levels of practicability, which are largely owing to the characteristics of an *in vitro* human BBB model introduced. Actual implementation of BBB/PBPK methods in drug development process is critically dependent on the credibility of *in vitro* BBB permeability parameters as surrogates for those found *in vivo*. Regarding this point, in this study we obtained *in vitro* Pe values using the hiBBB model and compared them with the *in vivo* BBB permeability (Q_{ECF}) of eight drugs estimated using an authentic top-down CNS-PBPK modeling approach. We can say, based on the results, that the correlation level between the Q_{ECF} and the Pe values is high enough to infer that, at least for the eight drugs, the hiBBB model can well recapitulate their *in vivo* BBB permeabilities and thus generally expected in other *in vitro* human BBB models as well (though the accuracy is dependent on the performance level of individual BBB model used). Although further discussion should await other studies using different types of *in vitro* human BBB models in future, these findings are considered likely to provide a rationale for development of a BBB/PBPK method.

Another key point to discuss with respect to *in vitro* human BBB models used in a BBB/PBPK method is that BMEC-based BBB models, like ours, are equipped with all the biological components that potentially affect human BBB permeability to drugs, among which influx and efflux transporters are particularly noteworthy. Early in the drug development process, it is quite difficult to evaluate the net effect of such transporter functions on drug BBB permeability even if the involvement of individual transporters is suspected based on other *in vitro* assays. However, use of an *in vitro* human BBB model may alleviate this confounding matter, as exemplified by gabapentin in this study. It has been reported that gabapentin is not only a substrate of an influx transporter (LAT1, (25)), but also a substrate of an efflux transporter (P-gp, (26)), which makes it difficult to easily assume its human BBB permeability. However, gabapentin turns out to have a relatively low BBB permeability in Fig. 4. This *in vitro* result is consistent with the fact that gabapentin is poorly distributed in the human brain (16) and with the low *in vivo* Q_{ECF} estimated in this study. Therefore, it is expected that *in vitro* human BBB models will provide adequate human BBB permeability data for use in a BBB/PBPK method, which would otherwise be difficult to obtain using data from individual transporter assays alone. It is also noteworthy that one-stop evaluation of BBB permeability of drugs with *in vitro* BBB models is overwhelmingly easier than several conventional approaches that require time and labor-intensive animal experiments or multiple transporter expression systems.

Taken together, our results presented in this study strongly encourage development of a BBB/PBPK method as a new approach to prediction of brain drug concentration profiles. Nevertheless, to increase reliability of a BBB/PBPK method, various challenges will need to be addressed, including quantification of transporter protein expression levels in *in vitro* human BBB models and refinement of CNS-PBPK modeling. But, the most prioritized challenge is the accumulation of IVIVC results regarding various types of drugs, particularly transporter substrate drugs, because prediction

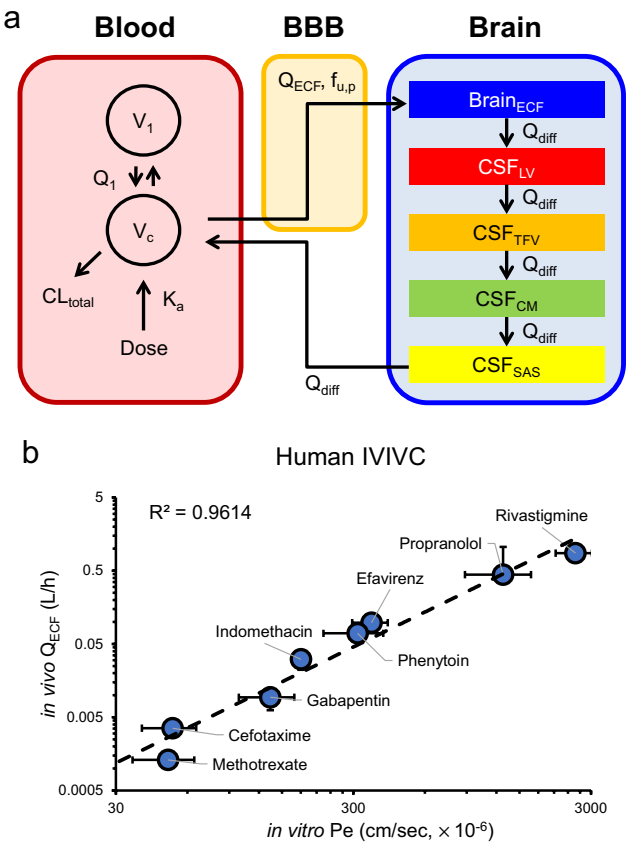

Fig. 5 Correlation analysis between *in vitro* Pe values obtained from the hiBBB model and *in vivo* Q_{ECF} estimated by CNS-PBPK modeling using human clinical data (**a**) The structure of the human CNS-PBPK model is shown. The model consists of two empirical compartments for the systemic circulation and five physiologically based compartments for the CNS. $Brain_{ECF}$, brain extracellular fluid (ECF); V_{LV}, volume of cerebrospinal fluid (CSF) in the lateral ventricle; V_{TFV}, volume of CSF in the third and fourth ventricle; V_{CM}, volume of CSF in the cisterna magna; V_{SAS}, volume of CSF in the subarachnoid space. (**b**) IVIVC using *in vitro* BBB permeability (Pe) obtained from the hiBBB models (x-axis) and *in vivo* brain permeability (Q_{ECF}) (y-axis) determined by CNS-PBPK modeling using human clinical data, is shown. The Pe values of propranolol used here had been determined in our previous study (7). The dashed line is generated by linear regression analysis with R^2 value.

of the brain concentrations of such drugs is extremely difficult. In this study, only three out of the eight drugs are classified as transporter substrates, which is apparently not enough for concrete evaluation of the applicability of a BBB/PBPK method to those drugs. Also, the methotrexate datapoint stands slightly away from the linear regression curve for a currently unclear reason. Therefore, despite considerable limitations, additional collection of IVIVC data on various types of drugs, including transporter substrates, further verifies the feasibility and effectiveness of a BBB/PBPK method. To be more accurate in these studies, it will be better to collect all relevant clinical information, not just brain concentration data, like sampling points, dosage timing, plasma drug concentration profiles, etc.

Finally, we would like to briefly mention the properties of the hiBBB model, which significantly contribute to the concept development of the BBB/PBPK method in this study. The hiBBB model is clearly able to discriminate between the seventeen drugs and compounds, and the dynamic range of their Pe values is comparable to those obtained by animal BBB models (27–29). These results are likely to be related to the fact that the hiBBB model possesses similar gene expression profiles, barrier properties, and efflux transporter functions to those of the hprBBB model. Therefore, while theoretically any type of *in vitro* human BBB models can be utilized, the hiBBB model may be a reasonable option for exploring the possibility of BBB/PBPK method implementation. Nevertheless, it should be borne in mind that its relatively weak barrier properties (e.g., claudin-5 mRNA levels of HBMEC/ci18 cells are lower than that of prHBMEC cells as shown in Fig. 1b) might pose a risk for overestimation or inaccuracy in BBB/PBPK prediction for drugs that enter the brain through paracellular routes. Therefore, continuous research efforts for improvement in hiBBB model functionality, including culture method optimization, to bridge the gaps between *in vitro* and *in vivo* will be necessary.

In conclusion, to the best of our knowledge, this is the first feasibility report toward the development of a BBB/PBPK method. While the number of drugs examined is limited, there is a significantly high level of correlation between the Q_{ECF} and the Pe values, indicating that *in vitro* human BBB models can provide valid BBB permeability parameters usable in a BBB/PBPK method. Therefore, our findings present a convincing rationale for development of the new method, which is expected to make an outstanding impact on CNS drug development through precise brain drug concentration prediction. We also hope that the hiBBB model will contribute to the story.

Supplementary Information The online version contains supplementary material available at https://doi.org/10.1007/s11095-022-03189-y.

Acknowledgements This work was supported by research funds from Eisai (Tokyo, Japan) and Ono Pharmaceuticals (Osaka, Japan), and partly by grants from JSPS KAKENHI (19K07214), and AMED under Grant Number JP17be0304322h0001. Otherwise, we have no financial relationship to disclose for this manuscript.

Declarations

Conflict of interest Conflict of interest statements related to research funds are provided in the acknowledgement section, and the model development method herein has been applied for a patent (No. 2020–065670). There is another related patent application (No. 2020–007041). The authors declare that they do not have any other conflicts of interest.

References

1. Cecchelli R, Berezowski V, Lundquist S, Culot M, Renftel M, Dehouck MP, et al. Modelling of the blood-brain barrier in drug discovery and development. Nat Rev Drug Discov. 2007;6(8):650–61.
2. Abbott NJ, Patabendige AAK, Dolman DEM, Yusof SR, Begley DJ. Structure and function of the blood-brain barrier. Neurobiol Dis. 2010;37(1):13–25.
3. Shimomura K, Okura T, Kato S, Couraud PO, Schermann JM, Terasaki T, Deguchi Y. Functional expression of a proton-coupled organic cation (H^+/OC) antiporter in human brain capillary endothelial cell line hCMEC/D3, a human blood-brain barrier model. Fluids Barriers CNS. 2013;26;10(1):8.
4. Yamamoto Y, Danhof M, de Lange ECM. Microdialysis: the Key to Physiologically Based Model Prediction of Human CNS Target Site Concentrations. AAPS J. 2017;19(4):891–909.
5. Uchida Y, Ohtsuki S, Katsukura Y, Ikeda C, Suzuki T, Kamiie J, et al. Quantitative targeted absolute proteomics of human blood-brain barrier transporters and receptors. J Neurochem. 2011;117(2):333–45.
6. Veszelka S, Tóth A, Walter FR, Tóth AE, Gróf I, Mészáros M, et al. Comparison of a Rat Primary Cell-Based Blood-Brain Barrier Model With Epithelial and Brain Endothelial Cell Lines: Gene Expression and Drug Transport. Front Mol Neurosci. 2018;11:166.
7. Ito R, Umehara K, Suzuki S, Kitamura K, Nunoya K, Yamaura Y, et al. A Human Immortalized Cell-Based Blood-Brain Barrier Triculture Model: Development and Characterization as a Promising Tool for Drug-Brain Permeability Studies. Mol Pharm. 2019;16(11):4461–71.
8. Furihata T, Ito R, Kamiichi A, Saito K, Chiba K. Establishment and characterization of a new conditionally immortalized human astrocyte cell line. J Neurochem. 2016;136(1):92–105.
9. Umehara K, Sun Y, Hiura S, Hamada K, Itoh M, Kitamura K, et al. A New Conditionally Immortalized Human Fetal Brain Pericyte Cell Line: Establishment and Functional Characterization as a Promising Tool for Human Brain Pericyte Studies. Mol Neurobiol. 2018;55(7):5993–6006.
10. Kitamura K, Ito R, Umehara K, Morio H, Saito K, Suzuki S, et al. Differentiated HASTR/ci35 cells: A promising *in vitro* human astrocyte model for facilitating CNS drug development studies. J Pharmacol Sci. 2018;137(4):350–8.
11. Kamiichi A, Furihata T, Kishida S, Ohta Y, Saito K, Kawamatsu S, et al. Establishment of a new conditionally immortalized cell line from human brain microvascular endothelial cells: a promising tool for human blood-brain barrier studies. Brain Res. 2012;1488:113–22.
12. Yamamoto Y, Välitalo PA, van den Berg DJ, Hartman R, van den Brink W, Wong YC, et al. A Generic Multi-Compartmental CNS Distribution Model Structure for 9 Drugs Allows Prediction of Human Brain Target Site Concentrations. Pharm Res. 2017;34(2):333–51.
13. Nau R, Prange HW, Muth P, Mahr G, Menck S, Kolenda H, et al. Passage of cefotaxime and ceftriaxone into cerebrospinal fluid of patients with uninflamed meninges. Antimicrob Agents Chemother. 1993;37(7):1518–24.
14. Best BM, Koopmans PP, Letendre SL, Capparelli EV, Rossi SS, Clifford DB, et al. Efavirenz concentrations in CSF exceed IC50 for wild-type HIV. J Antimicrob Chemother. 2011;66(2):354–7.
15. Mannila A, Kumpulainen E, Lehtonen M, Heikkinen M, Laisalmi M, Salo T, et al. Plasma and cerebrospinal fluid concentrations of indomethacin in children after intravenous administration. J Clin Pharmacol. 2007;47(1):94–100.
16. Ben-Menachem E, Persson LI, Hedner T. Selected CSF biochemistry and gabapentin concentrations in the CSF and plasma in patients with partial seizures after a single oral dose of gabapentin. Epilepsy Res. 1992;11(1):45–9.
17. Blakeley JO, Olson J, Grossman SA, He X, Weingart J, Supko JG, et al. Effect of blood brain barrier permeability in recurrent high grade gliomas on the intratumoral pharmacokinetics of methotrexate: a microdialysis study. J Neurooncol. 2009;91(1):51–8.
18. Gaohua L, Neuhoff S, Johnson TN, Rostami-Hodjegan A, Jamei M. Development of a permeability-limited model of the human brain and cerebrospinal fluid (CSF) to integrate known physiological and biological knowledge: Estimating time varying CSF drug concentrations and their variability using *in vitro* data. Drug Metab Pharmacokinet. 2016;31(3):224–33.
19. Taylor EA, Jefferson D, Carroll JD, Turner P. Cerebrospinal fluid concentrations of propranolol, pindolol and atenolol in man: evidence for central actions of beta-adrenoceptor antagonists. Br J Clin Pharmacol. 1981;12(4):549–59.
20. Gobburu JV, Tammara V, Lesko L, Jhee SS, Sramek JJ, Cutler NR, Yuan R. Pharmacokinetic-pharmacodynamic modeling of rivastigmine, a cholinesterase inhibitor, in patients with Alzheimer's disease. J Clin Pharmacol. 2001;41(10):1082–90.
21. Fridén M, Winiwarter S, Jerndal G, Bengtsson O, Wan H, Bredberg U, et al. Structure-brain exposure relationships in rat and human using a novel data set of unbound drug concentrations in brain interstitial and cerebrospinal fluids. J Med Chem. 2009;52(20):6233–43.
22. Paine SW, Ménochet K, Denton R, McGinnity DF, Riley RJ. Prediction of human renal clearance from preclinical species for a diverse set of drugs that exhibit both active secretion and net reabsorption. Drug Metab Dispos. 2011;39(6):1008–13.
23. Sadeghi K, Hadi F, Ahmadi A, Hamishehkar H, Beigmohammadi MT, Mahmoodpoor A, et al. Total Phenytoin concentration is not well correlated with active free drug in critically-ill head trauma patients. J Res Pharm Pract. 2013;2(3):105–9.
24. Evans GH, Nies AS, Shand DG. The disposition of propranolol. 3. Decreased half-life and volume of distribution as a result of plasma binding in man, monkey, dog and rat. J Pharmacol Exp Ther. 1973;186(1):114–22.
25. Dickens D, Webb SD, Antonyuk S, Giannoudis A, Owen A, Rädisch S, et al. Transport of gabapentin by LAT1 (SLC7A5). Biochem Pharmacol. 2013;85(11):1672–83.
26. Nakanishi H, Yonezawa A, Matsubara K, Yano I. Impact of P-glycoprotein and breast cancer resistance protein on the brain distribution of antiepileptic drugs in knockout mouse models. Eur J Pharmacol. 2013;710(1–3):20–8.
27. Marco AD, Paz OG, Fini I, Vignone D, Cellucci A, Battista MR, Auciello G, et al. Application of an *in Vitro* Blood-Brain Barrier Model in the Selection of Experimental Drug Candidates for the Treatment of Huntington's Disease. Mol Pharm. 2019;16(5):2069–82.
28. Lacombe O, Videau O, Chevillon D, Guyot AC, Contreras C, Blondel S, et al. *In vitro* primary human and animal cell-based blood-brain barrier models as a screening tool in drug discovery. Mol Pharm. 2011;8(3):651–63.
29. Nakagawa A, Deli MA, Kawaguchi H, Shimizudani T, Shimono T, Kittel A, et al. A new blood-brain barrier model using primary rat brain endothelial cells, pericytes and astrocytes. Neurochem Int. 2009;54(3–4):253–63.